Available online at www.sciencedirect.com
ScienceDirect
International Journal of Thermal Sciences 48 (2009) 34–49
International Journal of Thermal Sciences
www.elsevier.com/locate/ijts

A hyperbolic two-step model based finite difference scheme for studying thermal deformation in a double-layered thin film exposed to ultrashort-pulsed lasers

Tianchan Niu, Weizhong Dai *

Mathematics and Statistics, College of Engineering and Science, Louisiana Tech University, Ruston, LA 71272, USA

Received 1 August 2007; received in revised form 14 January 2008; accepted 4 February 2008

Available online 4 March 2008

Abstract

Hyperbolic two-step micro heat transport equations have attracted attention in thermal analysis of thin metal films exposed to ultrashort-pulsed lasers. In this article, we develop a finite difference scheme for studying thermal deformation in a 2D double-layered micro thin film exposed to ultrashort-pulsed lasers. This scheme is obtained based on the hyperbolic two-step model with temperature-dependent thermal properties coupled with the dynamic equations of motion. The method is illustrated by investigating thermal deformation in a gold layer on a chromium padding layer.

Keywords: Hyperbolic two-step model; Finite difference scheme; Ultrashort-pulsed laser; Thermal deformation

1. Introduction

Ultrashort-pulsed lasers with pulse durations of the order of sub-picosecond to femtosecond domain have the ability of limiting the undesirable spread of the thermal process zone in the heated sample [1]. They have been widely applied in structural monitoring of thin metal films [2], laser micromachining [3] and patterning [4], structural tailoring of microfilms [5], and laser synthesis and processing in thin-film deposition [6].

For an ultrashort-pulsed laser, the heating involves high-rate heat flow from electrons to lattices in the picosecond domains. The energy equations describing the continuous energy flow from hot electrons to lattices during non-equilibrium heating can be written as [7–9]:

$$C_e(T_e)\frac{\partial T_e}{\partial t} = \nabla\cdot\left[k_e(T_e,T_l)\nabla T_e\right] - G(T_e - T_l) + S \tag{1}$$

$$C_l\frac{\partial T_l}{\partial t} = G(T_e - T_l) \tag{2}$$

where $C_e(T_e) = A_e T_e$, $k_e(T_e, T_l) = k_0(T_e/T_l)$, T_e is electron temperature, T_l lattice temperature, k_0 thermal conductivity in thermal equilibrium, C_e and C_l volumetric heat capacity, G electron-lattice coupling factor, S laser heating source, and ∇ the gradient operator. Here, A_e, C_l, k_0 and G are all positive constants. The above coupled Eqs. (1) and (2), often referred to as parabolic two-step micro heat transport equations, have been widely applied in analysis of microscale heat transfer [7–17]. In particular, Wang et al. [18–20] developed a finite difference scheme based on the above model for studying thermal deformation in a two-dimensional thin film exposed to ultrashort-pulsed lasers. However, when the characteristic heating time (which is either the laser pulse during or the time needed to heat a material to a certain temperature) is much shorter than the electron relaxation time of free electrons (the mean time for electrons to change their states) in a metal, the parabolic two-step model may be inadequate to describe the continuous energy flow from hot electrons to lattices during non-equilibrium heating (see Fig. 1 in [11]). As Qiu and Tien [11] pointed out, the relaxation time increases dramatically, as the temperature decreases, from 0.04 ps at room temperature to about 10 ps at 10 K. They [9] developed the hyperbolic two-step heat transport equations based on the macroscopic averages of the electric

* Corresponding author. Tel.: +1 318 257 3301; fax: +1 318 257 2562.
E-mail address: dai@coes.latech.edu (W. Dai).

1290-0729/$ – see front matter
doi:10.1016/j.ijthermalsci.2008.02.001

Nomenclature

C_e	electron heat capacity	$\mathrm{J\,m^{-3}\,K^{-1}}$
C_l	lattice heat capacity	$\mathrm{J\,m^{-3}\,K^{-1}}$
G	electron-lattice coupling factor	$\mathrm{W\,m^{-3}\,K^{-1}}$
J	laser fluence	$\mathrm{J\,m^{-2}}$
K	bulk modulus	Pa
k_e	thermal conductivity	$\mathrm{W\,m^{-1}\,K^{-1}}$
L_x	length of micro thin film in the x-direction	μm
L_y	length of micro thin film in the y-direction	μm
N_x	number of grid points in the x-direction	
N_y	number of grid points in the y-direction	
q^x	heat flux in the x-direction	$\mathrm{W\,m^{-2}}$
q^y	heat flux in the y-direction	$\mathrm{W\,m^{-2}}$
R	surface reflectivity	
S	volumetric heat source	$\mathrm{W\,m^{-3}}$
T_e	electron temperature	K
T_l	lattice temperature	K
t	time	s
t_p	laser pulse duration	s
u	displacement in the x-direction	m
$u^n_{i,j}$	numerical solution of $u(x_i, y_j, t_n)$	
v	displacement in the y-direction	m
v_1	velocity component in the x-direction	$\mathrm{m\,s^{-1}}$
v_2	velocity component in the y-direction	$\mathrm{m\,s^{-1}}$
x, y	Cartesian coordinates	
x_s	optical penetration depth	m
y_s	spatial profile parameter	m

Greek symbols

α_T	thermal expansion coefficient	
$\Delta_{-t}, \delta_x, \delta_y$	finite difference operators	
∇_x, ∇_y	forward finite difference operators	
$\nabla_{\bar{x}}, \nabla_{\bar{y}}$	backward finite difference operators	
Δt	time increment	s
$\Delta x, \Delta y$	spatial grid sizes	m
ε	accuracy for convergence	
ε_x	normal strain in the x-direction	
ε_y	normal strain in the y-direction	
ε_{xy}	shear strain	
Λ	electron-blast coefficient	$\mathrm{J\,m^{-3}\,K^{-2}}$
λ	Lame's coefficients	Pa
μ	Lame's coefficients	Pa
ρ	density	$\mathrm{kg\,m^{-3}}$
σ_x	normal stress in the x-direction	Pa
σ_y	normal stress in the y-direction	Pa
σ_{xy}	shear stress	Pa
τ_e	electron relaxation time	ps
τ_l	lattice relaxation time	ps

Subscripts and superscripts

0	initial value at $t = 0$
e	electron
i	grid index in the x-direction
j	grid index in the y-direction
l	lattice
m	layer index
n	time level

and heat currents carried by electrons in the momentum space. Al-Nimr and his colleagues [21–25] also studied the thermal behavior of thin films using the hyperbolic two-step model. Chen and Beraun [26] proposed a generalized hyperbolic two-step model for studying ultrashort laser pulse interactions with metal films. The generalized hyperbolic two-step model can be written as follows [26–29]:

$$C_e\frac{\partial T_e}{\partial t} = -\nabla\cdot\vec{q_e} - G(T_e - T_l) + S \tag{3}$$

$$\tau_e\frac{\partial \vec{q_e}}{\partial t} + \vec{q_e} = -k_e\nabla T_e \tag{4}$$

$$C_l\frac{\partial T_l}{\partial t} = -\nabla\cdot\vec{q_l} + G(T_e - T_l) \tag{5}$$

$$\tau_l\frac{\partial \vec{q_l}}{\partial t} + \vec{q_l} = -k_l\nabla T_l \tag{6}$$

where $\vec{q_e}$ and $\vec{q_l}$ are the heat fluxes associated with the electrons and the lattice, respectively. Here, τ_e is the electron relaxation time of free electrons in metals, and τ_l is the lattice relaxation time in phonon collisions [26]. They are evaluated at the Fermi surface. A detailed description about τ_e can be seen in [30]. It can be seen that if τ_e, τ_l and k_l are zero, the hyperbolic two-step model will reduce to the parabolic two-step model. It should be pointed out that the heat conduction within the lattice domain usually has an insignificant effect compared to the conduction within the electron domain, because k_l is usually much smaller than k_e. For this case, Eq. (6) may be neglected.

In this study, we extend Wang et al.'s research [18–20] by developing an implicit finite difference scheme on a staggered grid based on the hyperbolic two-step model (Eqs. (3)–(6)) for studying thermal deformation in a two-dimensional double-layered thin film exposed to ultrashort-pulsed lasers. In particular, we employ our recently developed unconditionally stable finite difference scheme for solving the hyperbolic two-step model [31].

2. Governing equations

Consider a two-dimensional double-layered metal thin film exposed to ultrashort-pulsed lasers, as shown in Fig. 1(a). In Fig. 1(a), we assume that the thicknesses of these two layers are the same for simplicity. The governing equations for studying thermal deformation in the thin film include the dynamic equations of motion, the energy equations, the interfacial equation, and the initial and boundary conditions.

(1) *Dynamic equations of motion* [1]

$$\rho^{(m)}\frac{\partial^2 u^{(m)}}{\partial t^2} = \frac{\partial \sigma_x^{(m)}}{\partial x} + \frac{\partial \sigma_{xy}^{(m)}}{\partial y} + 2\Lambda^{(m)}T_e^{(m)}\frac{\partial T_e^{(m)}}{\partial x} \tag{7}$$

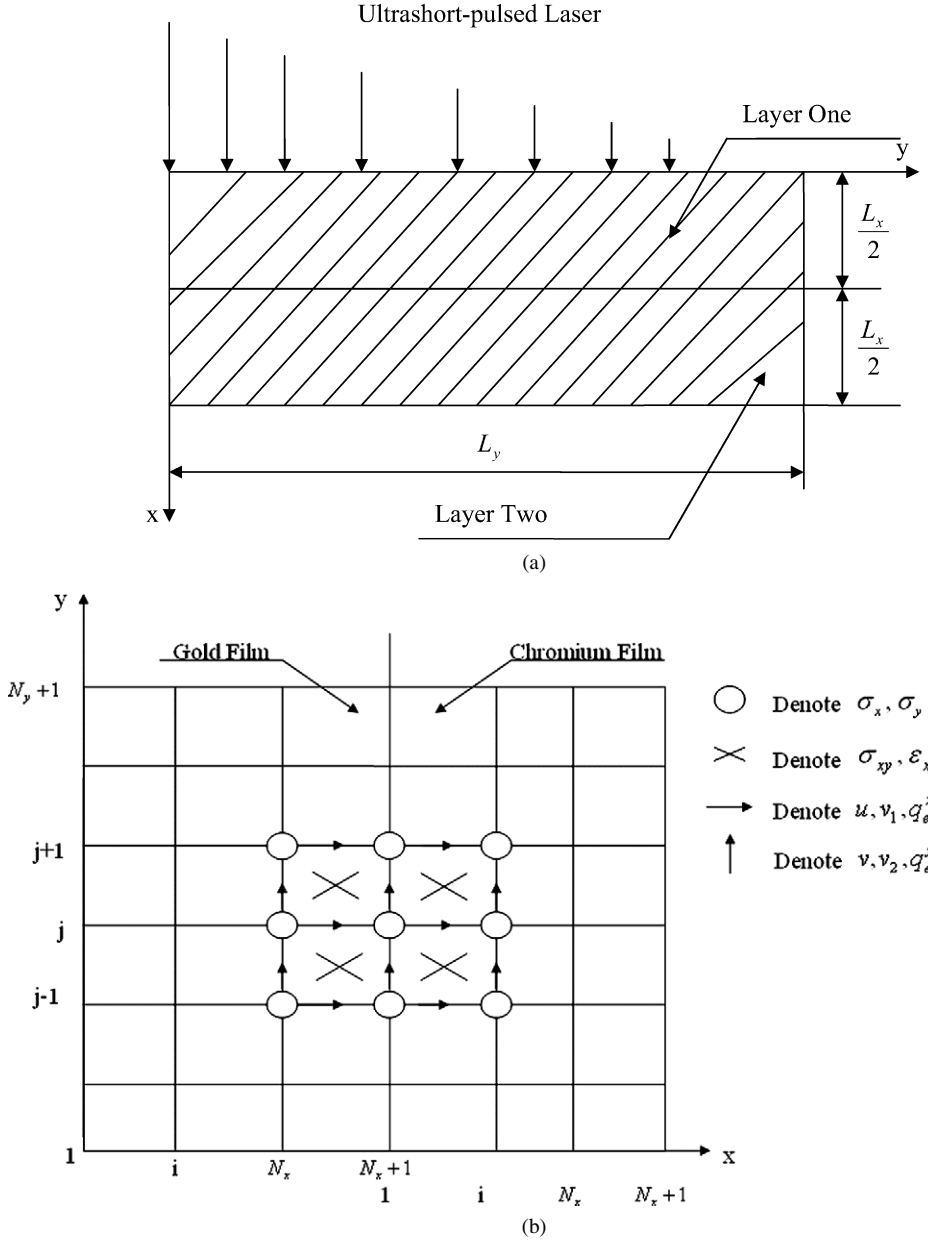

Fig. 1. (a) Configuration of a 2D double-layered thin film and (b) a staggered grid.

$$\rho^{(m)}\frac{\partial^2 v^{(m)}}{\partial t^2} = \frac{\partial \sigma_{xy}^{(m)}}{\partial x} + \frac{\partial \sigma_y^{(m)}}{\partial y} + 2\Lambda^{(m)} T_e^{(m)} \frac{\partial T_e^{(m)}}{\partial y} \tag{8}$$

where $\sigma_x^{(m)}$, $\sigma_y^{(m)}$, and $\sigma_{xy}^{(m)}$ are given by [27]

$$\sigma_x^{(m)} = \lambda^{(m)}\left(\varepsilon_x^{(m)} + \varepsilon_y^{(m)}\right) + 2\mu^{(m)}\varepsilon_x^{(m)} - \left(3\lambda^{(m)} + 2\mu^{(m)}\right)\alpha_T^{(m)}\left(T_l^{(m)} - T_0\right)$$

$$\sigma_y^{(m)} = \lambda^{(m)}\left(\varepsilon_x^{(m)} + \varepsilon_y^{(m)}\right) + 2\mu^{(m)}\varepsilon_y^{(m)} \tag{9}$$

$$- \left(3\lambda^{(m)} + 2\mu^{(m)}\right)\alpha_T^{(m)}\left(T_l^{(m)} - T_0\right) \tag{10}$$

$$\sigma_{xy}^{(m)} = \mu^{(m)}\varepsilon_{xy}^{(m)} \tag{11}$$

$$\varepsilon_x^{(m)} = \frac{\partial u^{(m)}}{\partial x}, \qquad \varepsilon_y^{(m)} = \frac{\partial v^{(m)}}{\partial y}, \qquad \varepsilon_{xy}^{(m)} = \frac{\partial u^{(m)}}{\partial y} + \frac{\partial v^{(m)}}{\partial x} \tag{12}$$

Here, $m = 1, 2$, denotes layer 1 and layer 2, respectively; $u^{(m)}$ is the displacement in the thickness direction (x-direction) and $v^{(m)}$ is the displacement in the length direction (y-direction); $\varepsilon_x^{(m)}$ and $\varepsilon_y^{(m)}$ are the normal strains in the x- and y-directions, respectively; $\varepsilon_{xy}^{(m)}$ is the shear strain; $\sigma_x^{(m)}$ and $\sigma_y^{(m)}$ are the normal stresses in the x- and y-directions, respectively; $\sigma_{xy}^{(m)}$ is the shear stress; $T_e^{(m)}$ and $T_l^{(m)}$ are electron and lattice temperatures, respectively; T_0 is an initial temperature; $\rho^{(m)}$ is density; $\Lambda^{(m)}$ is the electron-blast coefficient; $\lambda^{(m)}$ and $\mu^{(m)}$ are Lame's coefficients; and $\alpha_T^{(m)}$ is the thermal expansion coefficient.

(2) *Energy equations* [26–29]

$$C_e^{(m)}\frac{\partial T_e^{(m)}}{\partial t} = -\frac{\partial q_e^{x(m)}}{\partial x} - \frac{\partial q_e^{y(m)}}{\partial y} - G^{(m)}\left(T_e^{(m)} - T_l^{(m)}\right) + S \tag{13}$$

$$\tau_e^{(m)}\frac{\partial q_e^{x(m)}}{\partial t}+q_e^{x(m)}=-k_e^{(m)}\frac{\partial T_e^{(m)}}{\partial x} \tag{14}$$

$$\tau_e^{(m)}\frac{\partial q_e^{y(m)}}{\partial t}+q_e^{y(m)}=-k_e^{(m)}\frac{\partial T_e^{(m)}}{\partial y} \tag{15}$$

$$C_l^{(m)}\frac{\partial T_l^{(m)}}{\partial t}=-\frac{\partial q_l^{x(m)}}{\partial x}-\frac{\partial q_l^{y(m)}}{\partial x}+G^{(m)}\big(T_e^{(m)}-T_l^{(m)}\big)-\big(3\lambda^{(m)}+2\mu^{(m)}\big)\alpha_T^{(m)}T_0\frac{\partial}{\partial t}\big(\varepsilon_x^{(m)}+\varepsilon_y^{(m)}\big) \tag{16}$$

$$\tau_l^{(m)}\frac{\partial q_l^{x(m)}}{\partial t}+q_l^{x(m)}=-k_l^{(m)}\frac{\partial T_l^{(m)}}{\partial x} \tag{17}$$

$$\tau_l^{(m)}\frac{\partial q_l^{y(m)}}{\partial t}+q_l^{y(m)}=-k_l^{(m)}\frac{\partial T_l^{(m)}}{\partial y} \tag{18}$$

It is noted that we add the coupling effect between lattice temperature and strain rate in Eq. (16). In this study, the heat source introduced by [27] is extended for a Gaussian laser beam focusing at $y=0$ on the top surface as

$$S=0.94J\frac{1-R}{t_p x_s}\exp\left[-\frac{x}{x_s}-\left(\frac{y}{y_s}\right)^2-2.77\left(\frac{t-2t_p}{t_p}\right)^2\right] \tag{19}$$

Here, $\vec{q}_e^{\,(m)}=(q_e^{x(m)},q_e^{y(m)})$ and $\vec{q}_l^{\,(m)}=(q_l^{x(m)},q_l^{y(m)})$; J is laser fluence; R is surface reflectivity; t_p is laser pulse duration; x_s is optical penetration depth; y_s is spacial profile parameter.

The boundary conditions are assumed to be stress free [1,27] and no heat is lost from the surface in the short time response [32]:

$$\sigma_x^{(1)}=0,\quad \sigma_{xy}^{(1)}=0,\quad \text{at } x=0,\quad \text{and}$$
$$\sigma_x^{(2)}=0,\quad \sigma_{xy}^{(2)}=0\quad \text{at } x=L_x \tag{20a}$$

$$\sigma_y^{(1)}=0,\quad \sigma_{xy}^{(1)}=0,\quad \text{at } y=0,\quad \text{and}$$
$$\sigma_y^{(2)}=0,\quad \sigma_{xy}^{(2)}=0\quad \text{at } y=L_y \tag{20b}$$

$$\frac{\partial T_e^{(m)}}{\partial \vec{n}}=0,\quad \text{and}\quad \frac{\partial T_l^{(m)}}{\partial \vec{n}}=0 \tag{20c}$$

where $\vec{n}$ is the unit outward normal vector on the boundary.

The initial conditions are assumed to be

$$T_e^{(m)}=T_l^{(m)}=T_0,\qquad u^{(m)}=v^{(m)}=0$$
$$\frac{\partial u^{(m)}}{\partial t}=\frac{\partial v^{(m)}}{\partial t}=0,\quad \text{at } t=0 \tag{21}$$

where $m=1,2$. It is noted that the laser beam is applied on the top surface ($x=0$) at $t=0$ and the peak intensity occurs when $t=2t_p$.

The interfacial conditions are assumed to be those of perfect thermal contact at $x=L_x/2$ (the continuity of temperature and heat flux across the interface),

$$u^{(1)}=u^{(2)},\qquad v^{(1)}=v^{(2)} \tag{22a}$$
$$\sigma_x^{(1)}=\sigma_x^{(2)},\qquad \sigma_{xy}^{(1)}=\sigma_{xy}^{(2)} \tag{22b}$$
$$T_e^{(1)}=T_e^{(2)},\qquad q_e^{x(1)}=q_e^{x(2)} \tag{22c}$$
$$T_l^{(1)}=T_l^{(2)},\qquad q_l^{x(1)}=q_l^{x(2)} \tag{22d}$$

3. Finite difference scheme

To avoid non-physical oscillations in the solution, we follow the approach in [18–20,33] and introduce two velocity components $v_1^{(m)}$ and $v_2^{(m)}$ to the model. Thus, the dynamic equations of motion, Eqs. (7), (8), (11) and (12), can be rewritten as follows:

$$v_1^{(m)}=\frac{\partial u^{(m)}}{\partial t},\qquad v_2^{(m)}=\frac{\partial v^{(m)}}{\partial t} \tag{23}$$

$$\rho^{(m)}\frac{\partial v_1^{(m)}}{\partial t}=\frac{\partial \sigma_x^{(m)}}{\partial x}+\frac{\partial \sigma_{xy}^{(m)}}{\partial y}+\Lambda^{(m)}\frac{\partial (T_e^{(m)})^2}{\partial x} \tag{24}$$

$$\rho^{(m)}\frac{\partial v_2^{(m)}}{\partial t}=\frac{\partial \sigma_{xy}^{(m)}}{\partial x}+\frac{\partial \sigma_y^{(m)}}{\partial y}+\Lambda^{(m)}\frac{\partial (T_e^{(m)})^2}{\partial y} \tag{25}$$

$$\frac{\partial \varepsilon_x^{(m)}}{\partial t}=\frac{\partial v_1^{(m)}}{\partial x},\qquad \frac{\partial \varepsilon_y^{(m)}}{\partial t}=\frac{\partial v_2^{(m)}}{\partial y}$$
$$\frac{\partial \varepsilon_{xy}^{(m)}}{\partial t}=\frac{\partial v_1^{(m)}}{\partial y}+\frac{\partial v_2^{(m)}}{\partial x} \tag{26}$$

We then design a staggered grid, as shown in Fig. 1(b), where $v_1^{(m)}$, $q_e^{x(m)}$, $q_l^{x(m)}$ are placed at $(x_{i+\frac{1}{2}},y_j)$; $v_2^{(m)}$, $q_e^{y(m)}$, $q_l^{y(m)}$ are placed at $(x_i,y_{j+\frac{1}{2}})$; $\varepsilon_{xy}^{(m)}$ and $\sigma_{xy}^{(m)}$ are placed at $(x_{i+\frac{1}{2}},y_{j+\frac{1}{2}})$, while $\varepsilon_x^{(m)}$, $\varepsilon_y^{(m)}$, $\sigma_x^{(m)}$, $\sigma_y^{(m)}$, $T_e^{(m)}$ and $T_l^{(m)}$ are at (x_i,y_j). Here, i and j are indices with $1\leqslant i\leqslant N_x+1$ and $1\leqslant j\leqslant N_y+1$. $(T_e^{(m)})_{i,j}^n$, $(T_l^{(m)})_{i,j}^n$, $(q_e^{x(m)})_{i+\frac{1}{2},j}^n$, $(q_l^{x(m)})_{i+\frac{1}{2},j}^n$, $(q_e^{y(m)})_{i,j+\frac{1}{2}}^n$, $(q_l^{y(m)})_{i,j+\frac{1}{2}}^n$, $(v_1^{(m)})_{i+\frac{1}{2},j}^n$ and $(v_2^{(m)})_{i,j+\frac{1}{2}}^n$ are denoted as the numerical approximations of $T_e^{(m)}(i\Delta x,j\Delta y,n\Delta t)$, $T_l^{(m)}(i\Delta x,j\Delta y,n\Delta t)$, $q_e^{x(m)}((i+\frac{1}{2})\Delta x,j\Delta y,n\Delta t)$, $q_l^{x(m)}((i+\frac{1}{2})\Delta x,j\Delta y,n\Delta t)$, $q_e^{y(m)}(i\Delta x,(j+\frac{1}{2})\Delta y,n\Delta t)$, $q_l^{y(m)}(i\Delta x,(j+\frac{1}{2})\Delta y,n\Delta t)$, $v_1^{(m)}((i+\frac{1}{2})\Delta x,j\Delta y,n\Delta t)$ and $v_2^{(m)}(i\Delta x,(j+\frac{1}{2})\Delta y,n\Delta t)$, respectively, where Δt, Δx and Δy are time increment and spatial step sizes, respectively. Similar notations are used here for other variables. We further introduce the finite difference operators, Δ_{-t}, δ_x, δ_y, ∇_x, $\nabla_{\bar{x}}$, ∇_y, and $\nabla_{\bar{y}}$ as follows:

$$\Delta_{-t}u_{i,j}^n=u_{i,j}^n-u_{i,j}^{n-1}$$
$$\delta_x u_{i,j}^n=u_{i+\frac{1}{2},j}^n-u_{i-\frac{1}{2},j}^n,\qquad \delta_y u_{i,j}^n=u_{i,j+\frac{1}{2}}^n-u_{i,j-\frac{1}{2}}^n$$
$$\nabla_x u_{i,j}^n=\frac{u_{i+1,j}^n-u_{i,j}^n}{\Delta x},\qquad \nabla_{\bar{x}}u_{i,j}^n=\frac{u_{i,j}^n-u_{i-1,j}^n}{\Delta x}$$
$$\nabla_y u_{i,j}^n=\frac{u_{i,j+1}^n-u_{i,j}^n}{\Delta y},\qquad \nabla_{\bar{y}}u_{i,j}^n=\frac{u_{i,j}^n-u_{i,j-1}^n}{\Delta y}$$

Thus, Eqs. (24)–(26) are discretized using an implicit finite difference as follows:

$$\rho^{(m)}\frac{1}{\Delta t}\Delta_{-t}\big(v_1^{(m)}\big)_{i+\frac{1}{2},j}^{n+1}=\frac{1}{\Delta x}\delta_x\big(\sigma_x^{(m)}\big)_{i+\frac{1}{2},j}^{n+1}+\frac{1}{\Delta y}\delta_y\big(\sigma_{xy}^{(m)}\big)_{i+\frac{1}{2},j}^{n+1}+\Lambda^{(m)}\frac{1}{\Delta x}\delta_x\big[\big(T_e^{(m)}\big)^2\big]_{i+\frac{1}{2},j}^{n+1} \tag{27}$$

$$\rho^{(m)}\frac{1}{\Delta t}\Delta_{-t}\big(v_2^{(m)}\big)_{i,j+\frac{1}{2}}^{n+1} = \frac{1}{\Delta x}\delta_x\big(\sigma_{xy}^{(m)}\big)_{i,j+\frac{1}{2}}^{n+1} + \frac{1}{\Delta y}\delta_y\big(\sigma_y^{(m)}\big)_{i,j+\frac{1}{2}}^{n+1} + \Lambda^{(m)}\frac{1}{\Delta y}\delta_y\big[\big(T_e^{(m)}\big)^2\big]_{i,j+\frac{1}{2}}^{n+1} \tag{28}$$

$$\frac{1}{\Delta t}\Delta_{-t}\big(\varepsilon_x^{(m)}\big)_{i,j}^{n+1} = \frac{1}{\Delta x}\delta_x\big(v_1^{(m)}\big)_{i,j}^{n+1} \tag{29}$$

$$\frac{1}{\Delta t}\Delta_{-t}\big(\varepsilon_y^{(m)}\big)_{i,j}^{n+1} = \frac{1}{\Delta y}\delta_y\big(v_2^{(m)}\big)_{i,j}^{n+1} \tag{30}$$

$$\frac{1}{\Delta t}\Delta_{-t}\big(\varepsilon_{xy}^{(m)}\big)_{i+\frac{1}{2},j+\frac{1}{2}}^{n+1} = \frac{1}{\Delta x}\delta_x\big(v_2^{(m)}\big)_{i+\frac{1}{2},j+\frac{1}{2}}^{n+1} + \frac{1}{\Delta y}\delta_y\big(v_1^{(m)}\big)_{i+\frac{1}{2},j+\frac{1}{2}}^{n+1} \tag{31}$$

where $(\sigma_x^{(m)})_{i,j}^{n+1}$, $(\sigma_y^{(m)})_{i,j}^{n+1}$, and $(\sigma_{xy}^{(m)})_{i+\frac{1}{2},j+\frac{1}{2}}^{n+1}$ are obtained based on Eqs. (9)–(11)

$$\big(\sigma_x^{(m)}\big)_{i,j}^{n+1} = \lambda^{(m)}\big[\big(\varepsilon_x^{(m)}\big)_{i,j}^{n+1} + \big(\varepsilon_y^{(m)}\big)_{i,j}^{n+1}\big] + 2\mu^{(m)}\big(\varepsilon_x^{(m)}\big)_{i,j}^{n+1} - \big(3\lambda^{(m)} + 2\mu^{(m)}\big)\alpha_T^{(m)}\big[\big(T_l^{(m)}\big)_{i,j}^{n+1} - T_0\big] \tag{32}$$

$$\big(\sigma_y^{(m)}\big)_{i,j}^{n+1} = \lambda^{(m)}\big[\big(\varepsilon_x^{(m)}\big)_{i,j}^{n+1} + \big(\varepsilon_y^{(m)}\big)_{i,j}^{n+1}\big] + 2\mu^{(m)}\big(\varepsilon_y^{(m)}\big)_{i,j}^{n+1} - \big(3\lambda^{(m)} + 2\mu^{(m)}\big)\alpha_T^{(m)}\big[\big(T_l^{(m)}\big)_{i,j}^{n+1} - T_0\big] \tag{33}$$

$$\big(\sigma_{xy}^{(m)}\big)_{i+\frac{1}{2},j+\frac{1}{2}}^{n+1} = \mu^{(m)}\big(\varepsilon_{xy}^{(m)}\big)_{i+\frac{1}{2},j+\frac{1}{2}}^{n+1} \tag{34}$$

Further, Eqs. (13)–(18) are solved based on our recently developed finite difference scheme [31]:

$$A_e^{(m)}\frac{|(T_e^{(m)})_{i,j}^{n+1}|^3 - |(T_e^{(m)})_{i,j}^{n}|^3}{\frac{3}{2}\Delta t[(T_e^{(m)})_{i,j}^{n+1} + (T_e^{(m)})_{i,j}^{n}]} = -\nabla_{\bar{x}}\left[\frac{(q_e^{x(m)})_{i+\frac{1}{2},j}^{n+1} + (q_e^{x(m)})_{i+\frac{1}{2},j}^{n}}{2}\right] - \nabla_{\bar{y}}\left[\frac{(q_e^{y(m)})_{i,j+\frac{1}{2}}^{n+1} + (q_e^{y(m)})_{i,j+\frac{1}{2}}^{n}}{2}\right] - G^{(m)}\left[\frac{(T_e^{(m)})_{i,j}^{n+1} + (T_e^{(m)})_{i,j}^{n}}{2} - \frac{(T_l^{(m)})_{i,j}^{n+1} + (T_l^{(m)})_{i,j}^{n}}{2}\right] + S_{i,j}^{n+\frac{1}{2}} \tag{35}$$

$$\tau_e^{(m)}\frac{(q_e^{x(m)})_{i-\frac{1}{2},j}^{n+1} - (q_e^{x(m)})_{i-\frac{1}{2},j}^{n}}{\Delta t} + \frac{(q_e^{x(m)})_{i-\frac{1}{2},j}^{n+1} + (q_e^{x(m)})_{i-\frac{1}{2},j}^{n}}{2} = -\big(k_e^{(m)}\big)_{i-\frac{1}{2},j}^{n+\frac{1}{2}}\nabla_x\left[\frac{(T_e^{(m)})_{i,j}^{n+1} + (T_e^{(m)})_{i,j}^{n}}{2}\right] \tag{36}$$

$$\tau_e^{(m)}\frac{(q_e^{y(m)})_{i,j-\frac{1}{2}}^{n+1} - (q_e^{y(m)})_{i,j-\frac{1}{2}}^{n}}{\Delta t} + \frac{(q_e^{y(m)})_{i,j-\frac{1}{2}}^{n+1} + (q_e^{y(m)})_{i,j-\frac{1}{2}}^{n}}{2} = -\big(k_e^{(m)}\big)_{i,j-\frac{1}{2}}^{n+\frac{1}{2}}\nabla_y\left[\frac{(T_e^{(m)})_{i,j}^{n+1} + (T_e^{(m)})_{i,j}^{n}}{2}\right] \tag{37}$$

$$C_l^{(m)}\frac{(T_l^{(m)})_{i,j}^{n+1} - (T_l^{(m)})_{i,j}^{n}}{\Delta t} = -\nabla_{\bar{x}}\left[\frac{(q_l^{x(m)})_{i+\frac{1}{2},j}^{n+1} + (q_l^{x(m)})_{i+\frac{1}{2},j}^{n}}{2}\right] - \nabla_{\bar{y}}\left[\frac{(q_l^{y(m)})_{i,j+\frac{1}{2}}^{n+1} + (q_l^{y(m)})_{i,j+\frac{1}{2}}^{n}}{2}\right] + G^{(m)}\left[\frac{(T_e^{(m)})_{i,j}^{n+1} + (T_e^{(m)})_{i,j}^{n}}{2} - \frac{(T_l^{(m)})_{i,j}^{n+1} + (T_l^{(m)})_{i,j}^{n}}{2}\right] - \big(3\lambda^{(m)} + 2\mu^{(m)}\big)\alpha_T^{(m)}T_0\frac{\Delta_{-t}(\varepsilon_x^{(m)})_{i,j}^{n+1} + \Delta_{-t}(\varepsilon_y^{(m)})_{i,j}^{n+1}}{\Delta t} \tag{38}$$

$$\tau_l^{(m)}\frac{(q_l^{x(m)})_{i-\frac{1}{2},j}^{n+1} - (q_l^{x(m)})_{i-\frac{1}{2},j}^{n}}{\Delta t} + \frac{(q_l^{x(m)})_{i-\frac{1}{2},j}^{n+1} + (q_l^{x(m)})_{i-\frac{1}{2},j}^{n}}{2} = -k_l^{(m)}\nabla_x\left[\frac{(T_l^{(m)})_{i,j}^{n+1} + (T_l^{(m)})_{i,j}^{n}}{2}\right] \tag{39}$$

$$\tau_l^{(m)}\frac{(q_l^{y(m)})_{i,j-\frac{1}{2}}^{n+1} - (q_l^{y(m)})_{i,j-\frac{1}{2}}^{n}}{\Delta t} + \frac{(q_l^{y(m)})_{i,j-\frac{1}{2}}^{n+1} + (q_l^{y(m)})_{i,j-\frac{1}{2}}^{n}}{2} = -k_l^{(m)}\nabla_y\left[\frac{(T_l^{(m)})_{i,j}^{n+1} + (T_l^{(m)})_{i,j}^{n}}{2}\right] \tag{40}$$

where, in Eqs. (35) and (38), $2 \leqslant i \leqslant N_x$, $2 \leqslant j \leqslant N_y$ and $m = 1, 2$; in Eqs. (36) and (39), $1 \leqslant i \leqslant N_x$ and $2 \leqslant j \leqslant N_y$ when $m = 1$, and $1 \leqslant i \leqslant N_x - 1$ and $2 \leqslant j \leqslant N_y$ when $m = 2$; and in Eqs. (37) and (40), $2 \leqslant i \leqslant N_x$ and $1 \leqslant j \leqslant N_y$ when $m = 1$, and $1 \leqslant i \leqslant N_x - 1$ and $1 \leqslant j \leqslant N_y$ when $m = 2$. Here,

$$\big(k_e^{(m)}\big)_{i-\frac{1}{2},j}^{n+\frac{1}{2}} = \frac{1}{2}k_0^{(m)}\left|\frac{(T_e^{(m)})_{i,j}^{n+1} + (T_e^{(m)})_{i,j}^{n}}{(T_l^{(m)})_{i,j}^{n+1} + (T_l^{(m)})_{i,j}^{n}}\right| + \frac{1}{2}k_0^{(m)}\left|\frac{(T_e^{(m)})_{i-1,j}^{n+1} + (T_e^{(m)})_{i-1,j}^{n}}{(T_l^{(m)})_{i-1,j}^{n+1} + (T_l^{(m)})_{i-1,j}^{n}}\right|$$

and

$$\big(k_e^{(m)}\big)_{i,j-\frac{1}{2}}^{n+\frac{1}{2}} = \frac{1}{2}k_0^{(m)}\left|\frac{(T_e^{(m)})_{i,j}^{n+1} + (T_e^{(m)})_{i,j}^{n}}{(T_l^{(m)})_{i,j}^{n+1} + (T_l^{(m)})_{i,j}^{n}}\right| + \frac{1}{2}k_0^{(m)}\left|\frac{(T_e^{(m)})_{i,j-1}^{n+1} + (T_e^{(m)})_{i,j-1}^{n}}{(T_l^{(m)})_{i,j-1}^{n+1} + (T_l^{(m)})_{i,j-1}^{n}}\right|$$

It should be pointed out that the above nonlinear scheme, Eqs. (35)–(40) without the term $-(3\lambda^{(m)}+2\mu^{(m)})\alpha_T^{(m)}T_0\times(\Delta_{-t}(\varepsilon_x^{(m)})_{i,j}^{n+1}+\Delta_{-t}(\varepsilon_y^{(m)})_{i,j}^{n+1})/\Delta t$, is obtained based on an energy estimate for the energy equations and is shown to satisfy a discrete energy estimate without restriction on mesh ratio [31].

Once $v_1^{(m)}$ and $v_2^{(m)}$ are known, the displacements, $u^{(m)}$ and $v^{(m)}$, are obtained based on the Euler backward method for Eq. (23) as:

$$\frac{1}{\Delta t}\Delta_{-t}\big(u^{(m)}\big)_{i+\frac{1}{2},j}^{n+1}=\big(v_1^{(m)}\big)_{i+\frac{1}{2},j}^{n+1} \tag{41}$$

$$\frac{1}{\Delta t}\Delta_{-t}\big(v^{(m)}\big)_{i,j+\frac{1}{2}}^{n+1}=\big(v_2^{(m)}\big)_{i,j+\frac{1}{2}}^{n+1} \tag{42}$$

The boundary conditions, Eqs. (20a)–(20c), can be discretized as follows:

$$\big(\sigma_x^{(1)}\big)_{1,j}^{n}=0,\qquad \big(\sigma_x^{(2)}\big)_{N_x+1,j}^{n}=0$$
$$\big(\sigma_{xy}^{(1)}\big)_{\frac{3}{2},j+\frac{1}{2}}^{n+1}=0,\qquad \big(\sigma_{xy}^{(2)}\big)_{N_x+\frac{1}{2},j+\frac{1}{2}}^{n+1}=0,\quad 1\leqslant j\leqslant N_y \tag{43a}$$

$$\big(\sigma_y^{(1)}\big)_{i,1}^{n}=0,\qquad \big(\sigma_y^{(2)}\big)_{i,N_y+1}^{n}=0$$
$$\big(\sigma_{xy}^{(1)}\big)_{i+\frac{1}{2},\frac{3}{2}}^{n+1}=0,\qquad \big(\sigma_{xy}^{(2)}\big)_{i+\frac{1}{2},N_y+\frac{1}{2}}^{n+1}=0,\quad 1\leqslant i\leqslant N_x \tag{43b}$$

$$\big(T_e^{(1)}\big)_{1,j}^{n}=\big(T_e^{(1)}\big)_{2,j}^{n},\qquad \big(T_e^{(2)}\big)_{N_x+1,j}^{n}=\big(T_e^{(2)}\big)_{N_x,j}^{n}$$
$$1\leqslant j\leqslant N_y+1 \tag{43c}$$

$$\big(T_e^{(1)}\big)_{i,1}^{n}=\big(T_e^{(1)}\big)_{i,2}^{n},\qquad \big(T_e^{(2)}\big)_{i,N_y+1}^{n}=\big(T_e^{(2)}\big)_{i,N_y}^{n}$$
$$1\leqslant i\leqslant N_x+1 \tag{43d}$$

$$\big(T_l^{(1)}\big)_{1,j}^{n}=\big(T_l^{(1)}\big)_{2,j}^{n},\qquad \big(T_l^{(2)}\big)_{N_x+1,j}^{n}=\big(T_l^{(2)}\big)_{N_x,j}^{n}$$
$$1\leqslant j\leqslant N_y+1 \tag{43e}$$

$$\big(T_l^{(1)}\big)_{i,1}^{n}=\big(T_l^{(1)}\big)_{i,2}^{n},\qquad \big(T_l^{(2)}\big)_{i,N_y+1}^{n}=\big(T_l^{(2)}\big)_{i,N_y}^{n}$$
$$1\leqslant i\leqslant N_x+1 \tag{43f}$$

for any time level n. The initial conditions, Eq. (21), are discretized as

$$\big(u^{(m)}\big)_{i+\frac{1}{2},j}^{0}=0,\qquad \big(v^{(m)}\big)_{i,j+\frac{1}{2}}^{0}=0 \tag{44a}$$

$$\big(v_1^{(m)}\big)_{i+\frac{1}{2},j}^{0}=0,\qquad \big(v_2^{(m)}\big)_{i,j+\frac{1}{2}}^{0}=0 \tag{44b}$$

$$\big(T_e^{(m)}\big)_{i,j}^{0}=\big(T_l^{(m)}\big)_{i,j}^{0}=T_0 \tag{44c}$$

where $1\leqslant i\leqslant N_x+1$, $1\leqslant j\leqslant N_y+1$, and $m=1,2$.

Based on Eq. (22a), the interfacial conditions for velocity components $v_1^{(m)}$ and $v_2^{(m)}$ can be written as $v_1^{(1)}=v_1^{(2)}$ and $v_2^{(1)}=v_2^{(2)}$ on the interface. Thus, we assume that

$$\big(v_1^{(1)}\big)_{N_x+\frac{1}{2},j}^{n+1}=\big(v_1^{(2)}\big)_{\frac{3}{2},j}^{n+1},\qquad \big(v_2^{(1)}\big)_{N_x+\frac{1}{2},j}^{n+1}=\big(v_2^{(2)}\big)_{\frac{3}{2},j}^{n+1} \tag{45}$$

Using Eqs. (9)–(11), we discretize Eq. (22b) as follows:

$$\big(\lambda^{(1)}+2\mu^{(1)}\big)\big(\varepsilon_x^{(1)}\big)_{N_x+1,j}^{n+1}+\lambda^{(1)}\big(\varepsilon_y^{(1)}\big)_{N_x+1,j}^{n+1}-\big(3\lambda^{(1)}+2\mu^{(1)}\big)\alpha_T^{(1)}\big[\big(T_l^{(1)}\big)_{N_x+1,j}^{n+1}-T_0\big]$$
$$=\big(\lambda^{(2)}+2\mu^{(2)}\big)\big(\varepsilon_x^{(2)}\big)_{1,j}^{n+1}+\lambda^{(2)}\big(\varepsilon_y^{(2)}\big)_{1,j}^{n+1}-\big(3\lambda^{(2)}+2\mu^{(2)}\big)\alpha_T^{(2)}\big[\big(T_l^{(2)}\big)_{1,j}^{n+1}-T_0\big] \tag{46a}$$

$$\mu^{(1)}\big(\varepsilon_{xy}^{(1)}\big)_{N_x+\frac{1}{2},j+\frac{1}{2}}^{n+1}=\mu^{(2)}\big(\varepsilon_{xy}^{(2)}\big)_{\frac{3}{2},j+\frac{1}{2}}^{n+1} \tag{46b}$$

Eqs. (22c) and (22d) are discretized as

$$\big(T_e^{(1)}\big)_{N_x+1,j}^{n+1}=\big(T_e^{(2)}\big)_{1,j}^{n+1} \tag{47a}$$

$$\big(q_e^{x(1)}\big)_{N_x+\frac{1}{2},j}^{n+1}=\big(q_e^{x(2)}\big)_{\frac{3}{2},j}^{n+1} \tag{47b}$$

$$\big(T_l^{(1)}\big)_{N_x+1,j}^{n+1}=\big(T_l^{(2)}\big)_{1,j}^{n+1} \tag{47c}$$

$$\big(q_l^{x(1)}\big)_{N_x+\frac{1}{2},j}^{n+1}=\big(q_l^{x(2)}\big)_{\frac{3}{2},j}^{n+1} \tag{47d}$$

for any time level n and $1\leqslant j\leqslant N_y+1$.

Since the finite difference scheme (see Eqs. (27)–(28), (35)–(38)) is nonlinear, it must be solved by an iterative method. Here, the iterative method for solving the scheme at time level $n+1$ is described as follows:

Step 1. Guess $(\varepsilon_x^{(m)})^{n+1}$, $(\varepsilon_y^{(m)})^{n+1}$ and $(\varepsilon_{xy}^{(m)})^{n+1}$ by using the values of $(\varepsilon_x^{(m)})^{n}$, $(\varepsilon_y^{(m)})^{n}$ and $(\varepsilon_{xy}^{(m)})^{n}$. Obtain $(q_e^{x(m)})^{n+1}$, $(q_e^{y(m)})^{n+1}$, $(q_l^{x(m)})^{n+1}$and $(q_l^{y(m)})^{n+1}$ based on Eqs. (36), (37), (39), (40), and the interfacial conditions (46)–(47), and substitute them into Eqs. (35) and (38) to obtain $(T_e^{(m)})^{n+1}$ and $(T_l^{(m)})^{n+1}$.

Step 2. Solve Eqs. (32)–(34) for $(\sigma_x^{(m)})^{n+1}$, $(\sigma_y^{(m)})^{n+1}$ and $(\sigma_{xy}^{(m)})^{n+1}$.

Step 3. Solve Eqs. (27) and (28) for $(v_1^{(m)})^{n+1}$ and $(v_2^{(m)})^{n+1}$.

Step 4. Update $(\varepsilon_x^{(m)})^{n+1}$, $(\varepsilon_y^{(m)})^{n+1}$ and $(\varepsilon_{xy}^{(m)})^{n+1}$ by using Eqs. (29)–(31).

Given the required accuracy ϵ, repeat the above steps until a convergent solution is obtained based on the following criteria

$$\max\big|\big(\varepsilon_x^{(m)}\big)^{n+1(\text{new})}-\big(\varepsilon_x^{(m)}\big)^{n+1(\text{old})}\big|\leqslant\epsilon$$
$$\max\big|\big(\varepsilon_y^{(m)}\big)^{n+1(\text{new})}-\big(\varepsilon_y^{(m)}\big)^{n+1(\text{old})}\big|\leqslant\epsilon \tag{48a}$$
$$\max\big|\big(\varepsilon_{xy}^{(m)}\big)^{n+1(\text{new})}-\big(\varepsilon_{xy}^{(m)}\big)^{n+1(\text{old})}\big|\leqslant\epsilon \tag{48b}$$

Step 5. Solve Eqs. (41) and (42) for $(u^{(m)})^{n+1}$ and $(v^{(m)})^{n+1}$.

4. Numerical examples

To demonstrate the applicability of our present scheme, we considered a two-dimensional double-layered thin film, which is a gold layer on a chromium padding layer with the dimensions 0.05 μm (thickness) × 1 μm (length) each layer. The thermophysical properties for gold and chromium are listed in Table 1 [29,32,34,35].

In order to test the convergence of the scheme, three different meshes (80 × 40, 160 × 80, 200 × 100 for each layer) were chosen. The time increment is 0.005 ps. The required accuracy ϵ was chosen to be 10^{-16} for convergence. The initial temperature T_0 was chosen to be 300 K. In our computation, we chose $R=0.93$, $t_p=0.1\times10^{-12}$ s, $x_s=15.3\times10^{-9}$ m,

Table 1
Thermal properties for gold and chromium [29,32,34,35]

Parameter	Unit	Gold	Chromium
ρ	$\mathrm{kg\,m^{-3}}$	19300	7190
Λ	$\mathrm{J\,m^{-3}\,K^{-2}}$	70	193.3
λ	Pa	199×10^9	83.3×10^9
μ	Pa	27×10^9	115×10^9
α_T	$\mathrm{K^{-1}}$	14.2×10^{-6}	4.9×10^{-6}
A_e	$\mathrm{J\,m^{-3}\,K^{-2}}$	70	193.3
C_l	$\mathrm{J\,m^{-3}K^{-1}}$	2.5×10^6	3.3×10^6
G	$\mathrm{W\,m^{-3}K^{-1}}$	2.6×10^{16}	42×10^{16}
τ_e	ps	0.04	0.0068
τ_l	ps	0.8	0.136
k_0, k_l	$\mathrm{W\,m^{-1}K^{-1}}$	315	94

$y_s = 1.0 \times 10^{-6}$ m, and $J = 500.0\ \mathrm{J\,m^{-2}}$, $1000.0\ \mathrm{J\,m^{-2}}$ and $2000.0\ \mathrm{J\,m^{-2}}$, respectively.

Fig. 2(a) shows the change in electron temperature $(\Delta T_e/(\Delta T_e)_{\max})$ at $x = 0$ and $y = 0$ versus time for various meshes (80×40, 160×80, 200×100 for each layer) with laser fluence $J = 500\ \mathrm{J\,m^{-2}}$. The maximum electron temperature rise, $(\Delta T_e)_{\max}$, is about 3930 K. The electron temperature (3807 K) at $t = 0.3$ ps is close to 3727 K at $t = 0.1$ ps (starting at $t = -0.2$ ps), which was obtained by Tzou et al. [1] who employed a parabolic two-step model. We also compared the change in temperature on the surface of the gold layer with that obtained using the parabolic two-step model [19]. There is a slight difference between the hyperbolic model and the parabolic model. In particular, the hyperbolic model predicts a low temperature after the peak. This difference probably comes from the effect of relaxation times τ_e and τ_l, which needs further study. Fig. 2(b) shows the displacement (u) at $x = 0$ and $y = 0$ versus time for various meshes (80×40, 160×80, 200×100 for each layer). The figure also shows a slight difference between hyperbolic model and parabolic model. From both Figs. 2(a) and 2(b), it can be seen that grid size has no significant effect on the solution, implying the solution is convergent.

Figs. 3 and 4 show, respectively, the electron temperature (T_e) and lattice temperature (T_l) at $y = 0$ μm versus x (the thickness) with three different laser fluences ($J = 500\ \mathrm{J\,m^{-2}}$, $1000\ \mathrm{J\,m^{-2}}$ and $2000\ \mathrm{J\,m^{-2}}$) at various times (a) $t = 0.25$ ps, (b) $t = 0.5$ ps, (c) $t = 1.0$ ps, and (d) $t = 20$ ps. It can be seen from Fig. 3 that the electron temperature reaches its maximum at $t = 0.25$ ps, then decays with time and almost uniforms at $t = 20$ ps along the thickness direction. On the other hand, Fig. 4 shows that the lattice temperature increases gradually with time in both gold and chromium layers, due to constant heating of acoustic phonons by electrons. Since the heat is transferred from the gold layer to the chromium layer and the conductivity of chromium is smaller than that of gold, the lattice temperature increases drastically across the interface. Differing from that predicted by the parabolic two-step model in [1] or [19], the hyperbolic model does not predict a clear discontinuity of the temperature gradient at the interface as shown in Fig. 4 (b)–(d). This is probably because of the effect of relaxation time τ_l, as seen in Eq. (17). The difference of electron and lattice temperatures at $t = 0.25$ ps, $t = 0.5$ ps, and $t = 1.0$ ps in Figs. 3 and 4 gives a strong flavor of non-equilibrium heating during the picosecond transient. At $t = 20$ ps as shown in Figs. 3(d) and 4(d), there is no significant difference between electron temperature and lattice temperature, implying that the heating reaches an equilibrium state.

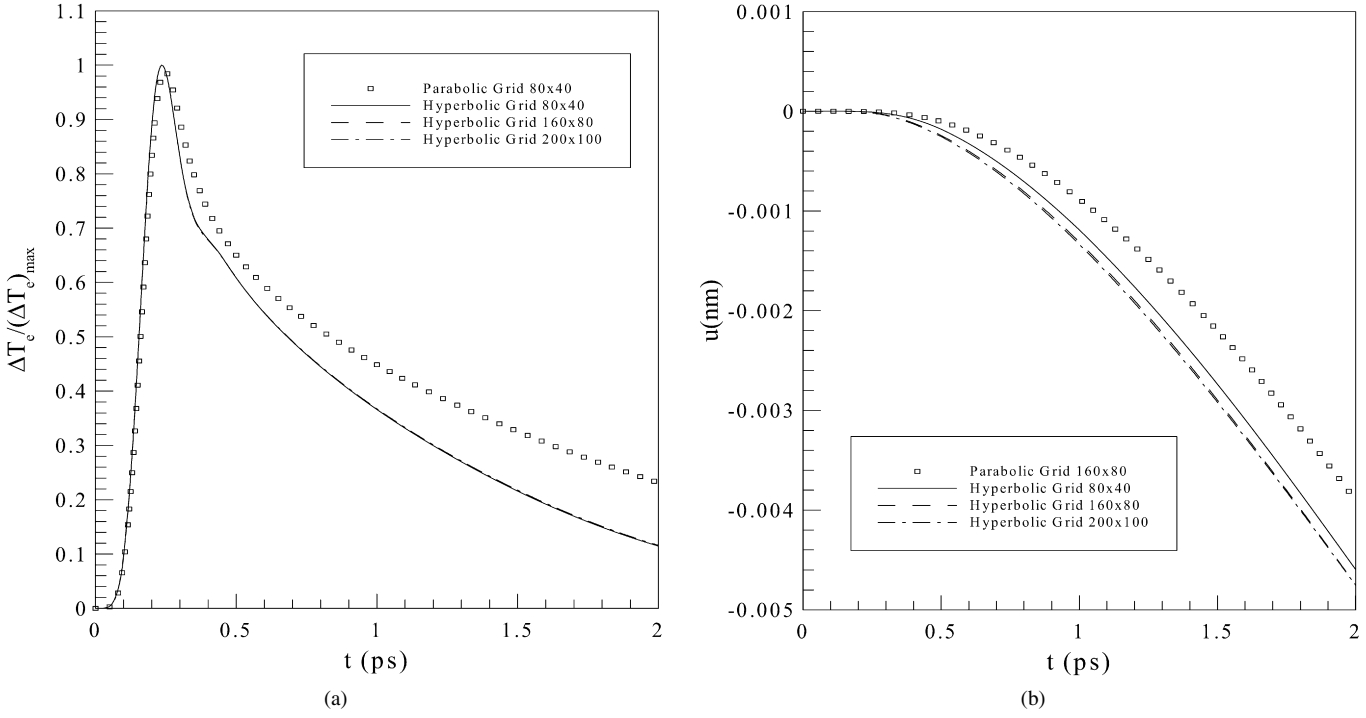

Fig. 2. (a) Change in electron temperature at $x = 0$ and $y = 0$, and (b) displacement (u) versus time for various meshes compared with parabolic two-step model [19].

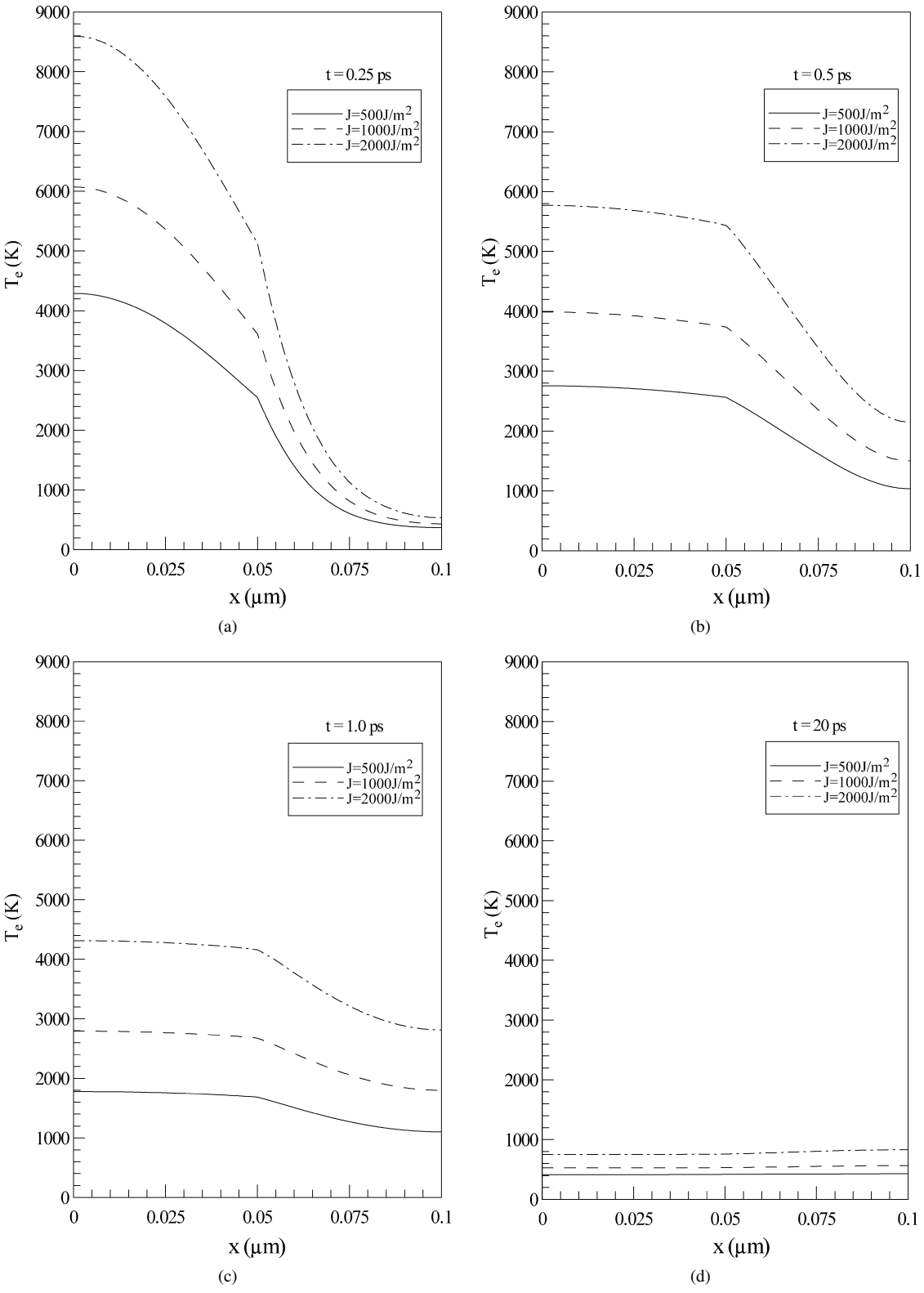

Fig. 3. Electron temperature (T_e) at $y = 0$ μm versus x at various times (a) $t = 0.25$ ps, (b) $t = 0.5$ ps, (c) $t = 1.0$ ps, and (d) $t = 20$ ps.

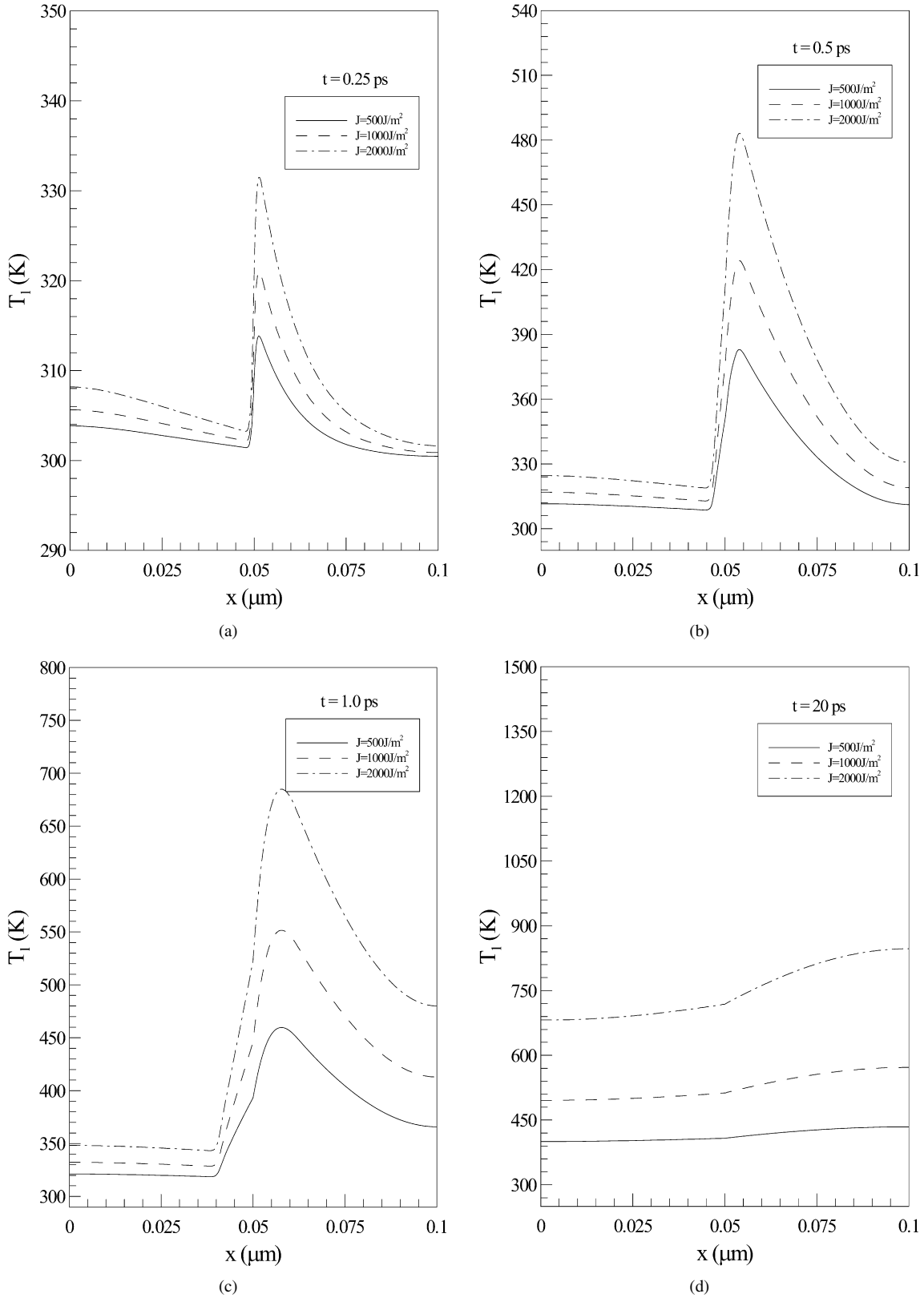

Fig. 4. Lattice temperature (T_l) at $y = 0$ μm versus x at various times (a) $t = 0.25$ ps, (b) $t = 0.5$ ps, (c) $t = 1.0$ ps, and (d) $t = 20$ ps.

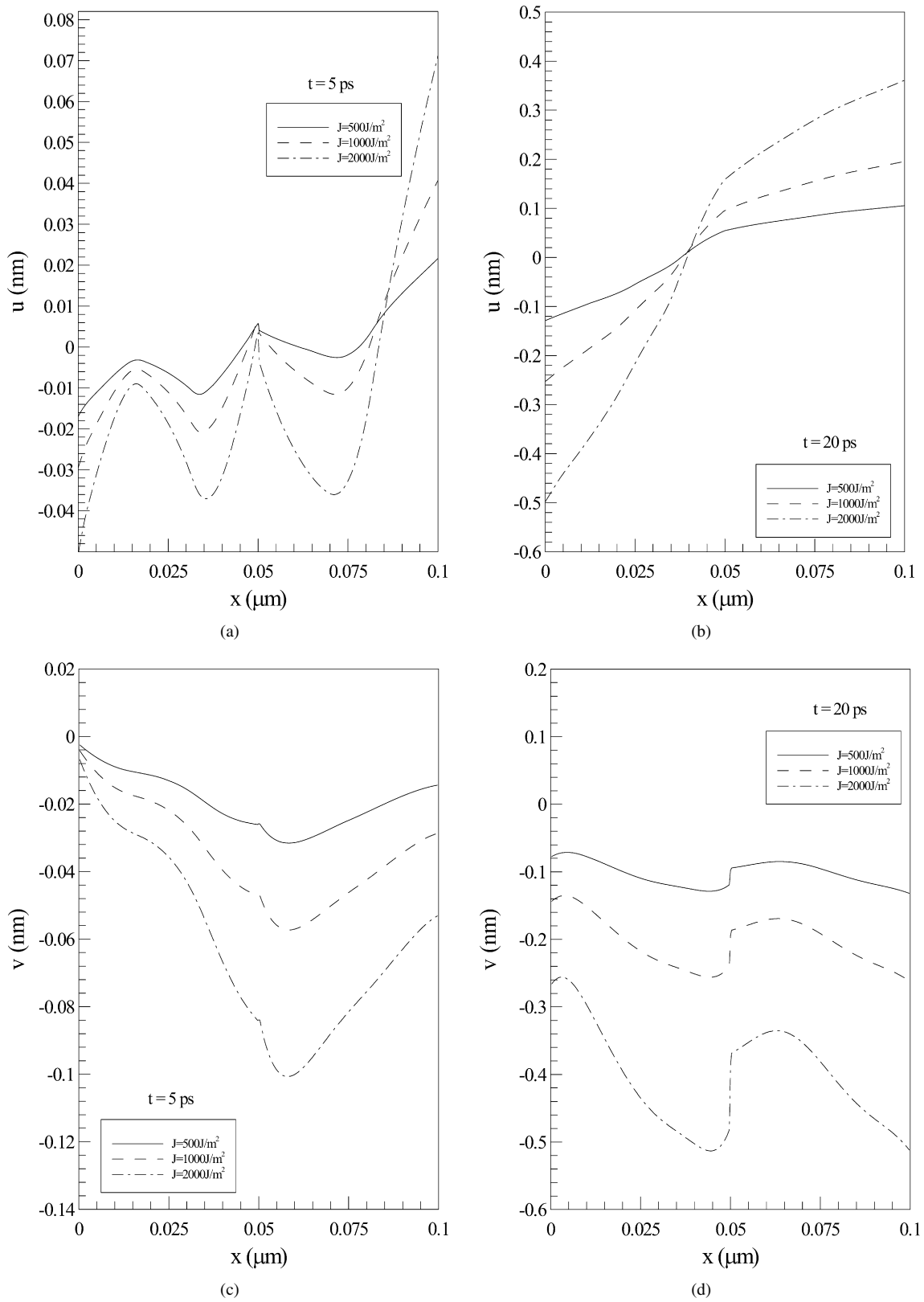

Fig. 5. Displacement (u) at $y = 0$ μm versus x at (a) $t = 5$ ps and (b) $t = 20$ ps, and displacement (v) at $y = 0$ μm versus x at (c) $t = 5$ ps and (d) $t = 20$ ps.

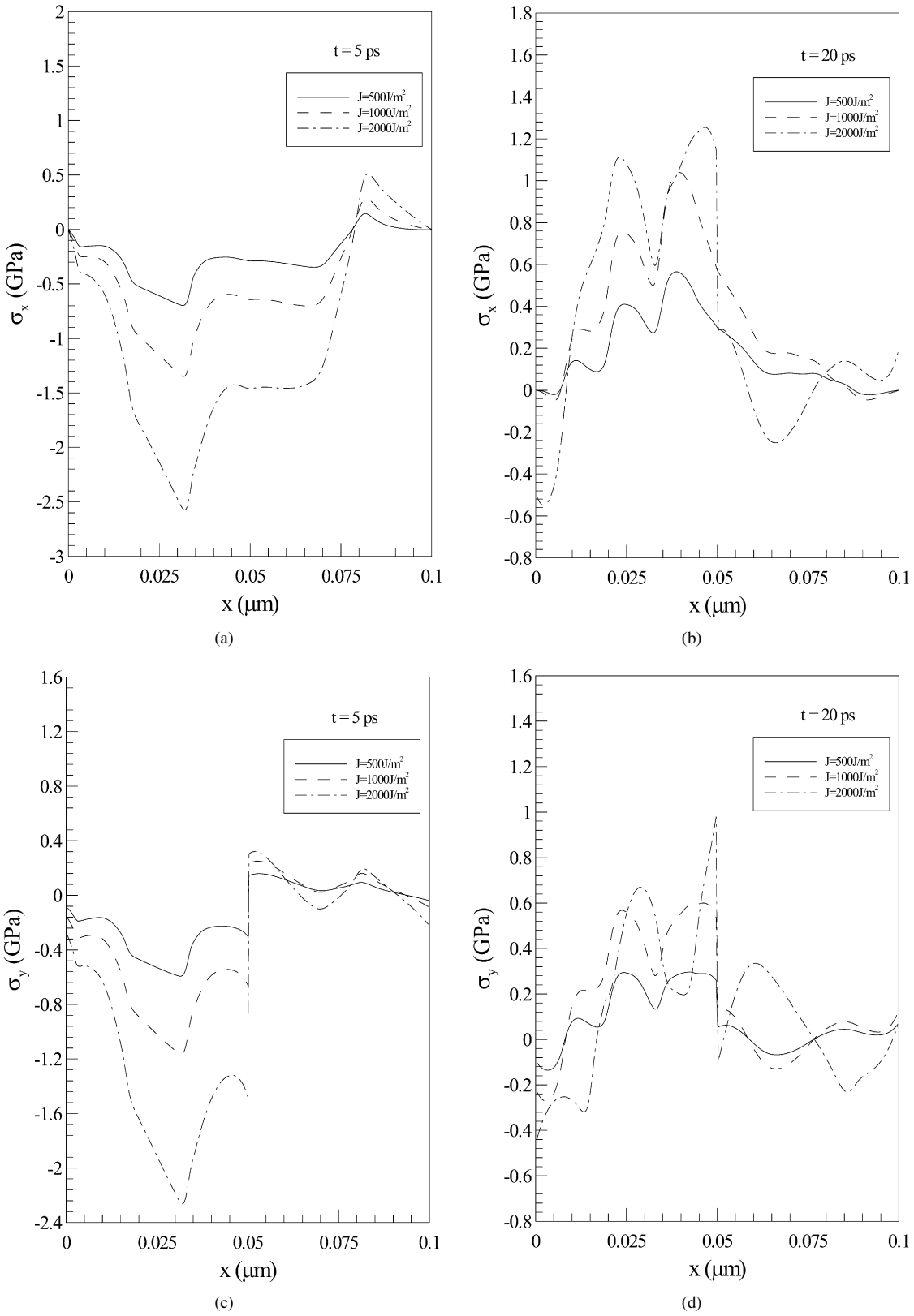

Fig. 6. Normal stress (σ_x) at $y = 0$ μm versus x at (a) $t = 5$ ps and (b) $t = 20$ ps, and normal stress (σ_y) versus x at $y = 0$ μm at (c) $t = 5$ ps, and (d) $t = 20$ ps.

Fig. 5 shows displacements u (thickness direction) and v (length direction) at $y = 0$ μm along x (the thickness) with three different laser fluences ($J = 500$ J m^{-2}, 1000 J m^{-2} and 2000 J m^{-2}) at various times $t = 5$ ps and $t = 20$ ps. It can been seen that the displacement u, particularly at $t = 20$ ps, changes from negative value to positive value along the thickness direction. It shows that most of the gold layer is expanding in the negative x direction while the chromium layer expands in the x-direction. On the other hand, the value of the displacement v is negative, implying that the film is expanding to the negative x-direction. At $t = 20$ ps, the displacement v shows a clear jump at the interface, implying that the bond between these two layers could be broken and could slip under a high intense laser irradiation. Fig. 5 also shows that the expansion of the film will be larger with increase of the laser fluency.

Fig. 6 shows normal stresses σ_x (thickness direction) and σ_y (length direction) at $y = 0$ μm along x with three different laser fluences ($J = 500$ J m^{-2}, 1000 J m^{-2} and 2000 J m^{-2}) at various times $t = 5$ ps and $t = 20$ ps. At $t = 5$ ps normal stress σ_x changes from negative to positive along the thickness direction, implying that the film is expanding. At $t = 20$ ps σ_x appears to be a wave-like curve along the thickness in the gold layer. The reason is probably due to the effect of the double layers. On the other hand, normal stress σ_y shows a jump across the interface because of different layers. Similar wave-like curve can be seen in σ_y at $t = 20$ ps. From our experience, the conventional finite difference method produces local oscillations in the normal stress σ_x. Chen et al. [27] employed successfully an artificial viscosity to suppress spurious oscillations for an axisymmetric thin film case under cylindrical coordinate system. We tried this approach to a 2D gold thin film under Cartesian coordinates. Unfortunately, the normal stress σ_x shows spurious oscillations, as compared with the solutions obtained based on our present method and Wang et al.'s parabolic two-step model based finite difference method [18], as shown in Fig. 7. It can be seen from Fig. 6 that the curve of σ_x is smooth and does not appear local oscillations, implying that our method prevents the appearance of non-physical oscillation in the solution.

Figs. 8 and 9 show the contours of electron temperature (T_e) and lattice temperature (T_l) with the laser fluence of $J = 1000$ J m^{-2} at various times (a) $t = 0.25$ ps, (b) $t = 0.5$ ps, (c) $t = 1.0$ ps, (d) $t = 10$ ps, respectively. It can be seen that the hot temperature changes from the top left corner to the bottom left corner in the double-layered thin film, implying that the heat is mainly transferred from the gold layer to the chromium layer along the x-direction. The contours of lattice temperature in the chromium layer are much brighter near the interface when $t = 0.25$ ps and $t = 0.5$ ps. This indicates that there is a larger temperature difference between the gold layer and the chromium layer across the interface. However, the difference gradually disappears as the heat is transferred to the bottom of the chromium layer as shown in Figs. 9(c) and 8(d).

Fig. 10 shows the contours of displacement u (thickness direction) and displacement v (length direction) with the laser influence of $J = 1000$ J m^{-2} at $t = 20$ ps. It can be seen from Fig. 10 that the film expands after heating because displacement changes from negative to positive along the x- and y-directions, respectively.

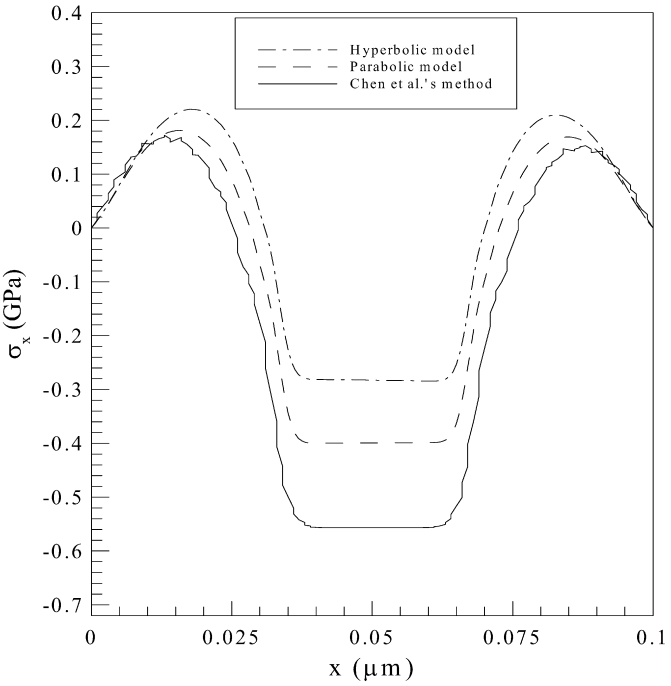

Fig. 7. Comparison of normal stress (σ_x) at $y = 0$ μm versus x at $t = 10$ ps obtained based on the present method, Wang et al.'s method [18] and Chen et al.'s method [27].

5. Conclusion

In this study, we have developed an implicit finite difference scheme for studying thermal deformation in a two-dimensional double-layered thin film exposed to ultrashort-pulsed lasers. The scheme is obtained based on the hyperbolic two-step heat transport equations (accounting for the coupling effect between lattice temperature and strain rate, as well as for the hot-electron blast effect in momentum transfer), and by replacing the displacement components in the dynamic equations of motion with the velocity components and constructing a staggered grid. The method is then applied to studying thermal deformation in a two-dimensional gold layer on a chromium padding layer exposed to ultrashort-pulsed lasers. Numerical results show the difference between the hyperbolic two-step model and parabolic two-step model, and the displacement alterations along x- and y-directions (which reveals the expansion of the thin film).

Further research will study the hyperbolic "physics" effects (such as changing laser heating duration, relaxation times, and diffusion in lattice) and the non-perfect thermal contact case (which will generate additional nonlinear behavior in the interfacial area).

Acknowledgements

The authors thank the referees for their valuable suggestions and comments.

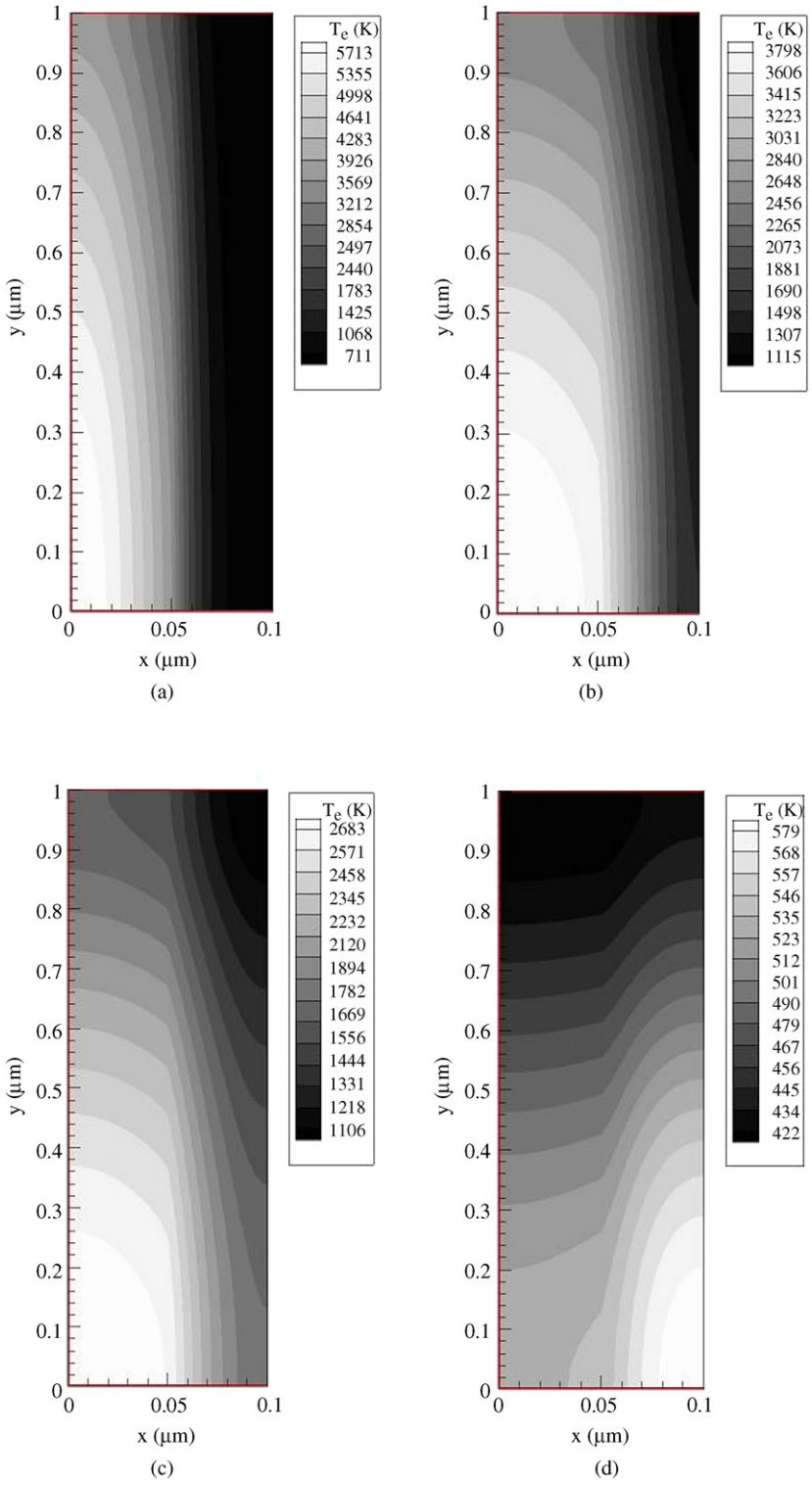

Fig. 8. Contours of electron temperature distributions at (a) $t = 0.25$ ps, (b) $t = 0.5$ ps, (c) $t = 1.0$ ps, and (d) $t = 10$ ps with $J = 1000\ \mathrm{J\,m^{-2}}$.

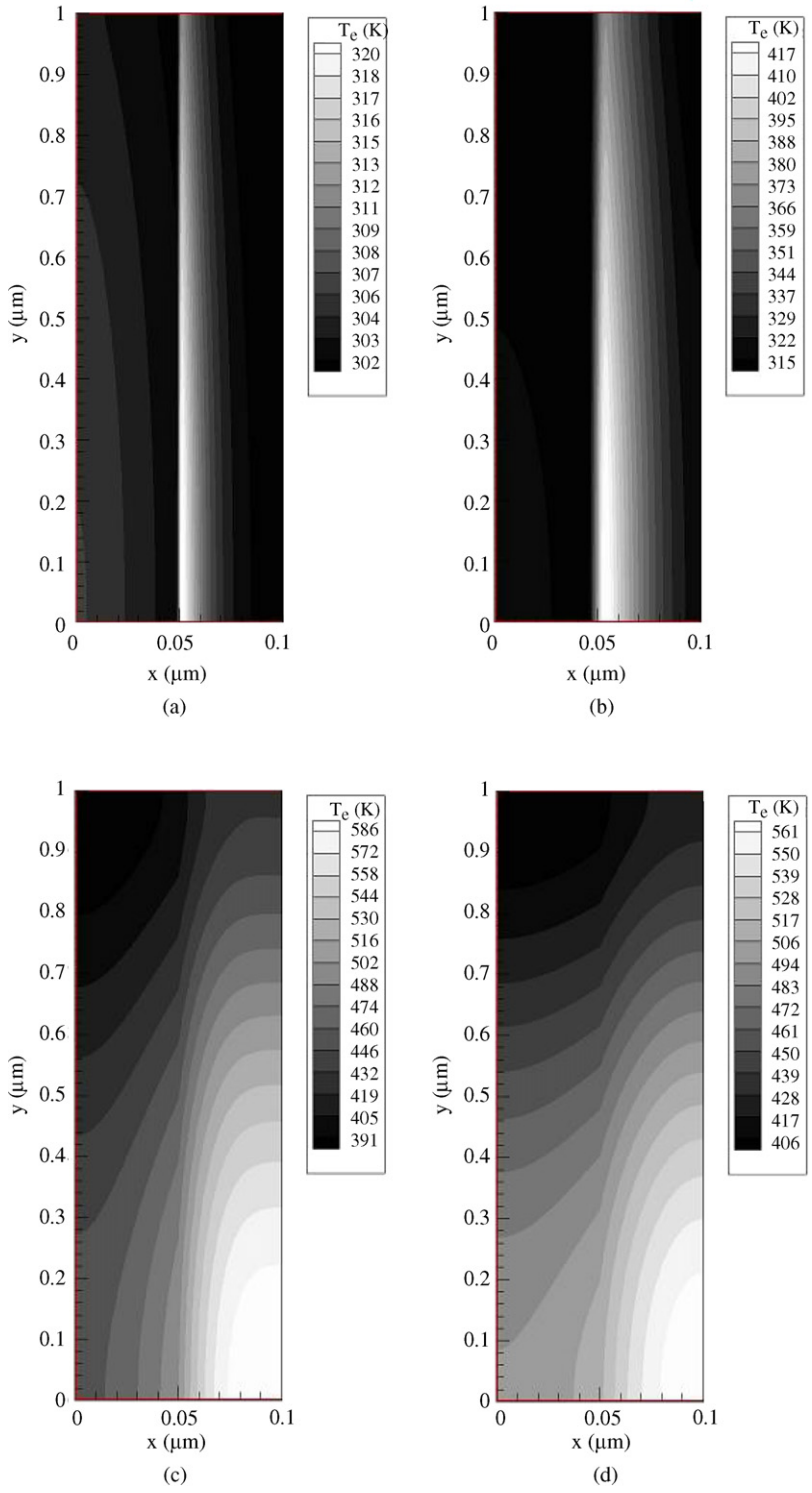

Fig. 9. Contours of lattice temperature distributions at (a) $t = 0.25$ ps, (b) $t = 0.5$ ps, (c) $t = 1.0$ ps, and (d) $t = 10$ ps with $J = 1000\ \mathrm{J\,m^{-2}}$.

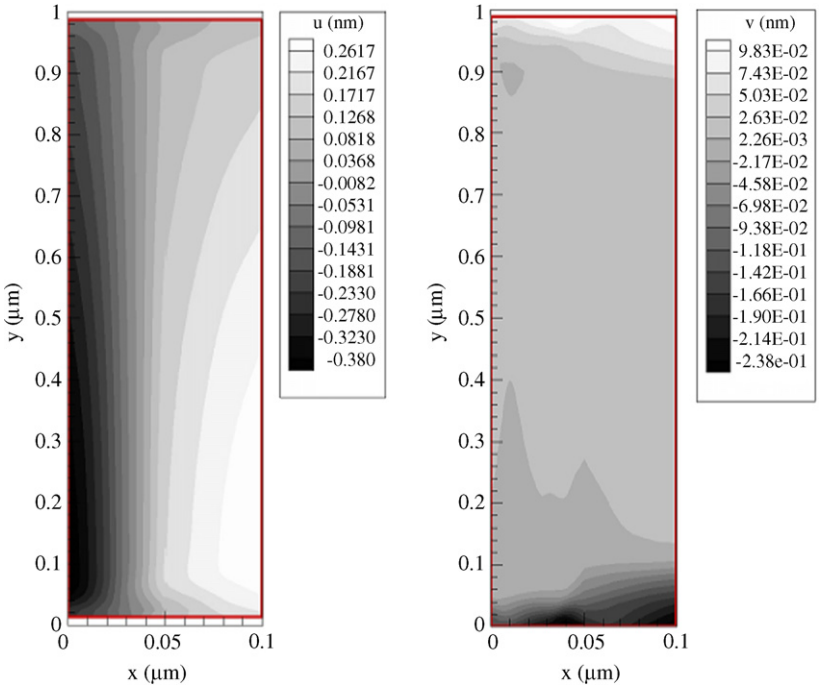

Fig. 10. Contours of displacements u and v distributions at $t = 20$ ps with $J = 1000\ \mathrm{J\,m^{-2}}$.

References

[1] D.Y. Tzou, J.K. Chen, J.E. Beraun, Hot-electron blast induced by ultrashort-pulsed lasers in layered media, Int. J. Heat Mass Transfer 45 (2002) 3369–3382.

[2] J. Opsal, The application of thermal wave technology to thickness and grain size of aluminum films, SPIE 1596 (1991) 120–131.

[3] J.A. Knapp, P. Borgesen, R.A. Zuhr, Beam-solid interactions: physical phenomena, Mater. Res. Soc. Symp. Proc. 157 (1990).

[4] D.J. Elliot, B.P. Piwczyk, Single and multiple pulse ablation of polymeric and high density materials with excimer laser radiation at 193 nm and 248 nm, Mater. Res. Soc. Symp. Proc. 129 (1989) 627–636.

[5] C.P. Grigoropoulos, Heat transfer in laser processing of thin films, in: Annual Review of Heat Transfer V, Hemisphere, New York, 1994.

[6] J. Narayan, V.P. Gosbole, G.W. White, Laser method for synthesis and processing of continuous diamond films on nondiamond substrates, Science 252 (1991) 416–418.

[7] S.I. Anisimov, B.L. Kapeliovich, T.L. Perel'man, Electron emission from metal surfaces exposed to ultrashort laser pulses, Sov. Phys. JETP 39 (1974) 375–377.

[8] T.Q. Qiu, C.L. Tien, Short-pulse laser heating on metals, Int. J. Heat Mass Transfer 35 (1992) 719–726.

[9] T.Q. Qiu, C.L. Tien, Heat transfer mechanisms during short-pulse laser heating of metals, ASME J. Heat Transfer 115 (1993) 835–841.

[10] A.N. Smith, J.L. Hosteler, P.M. Norris, Nonequilibrium heating in metal films: an analytical and numerical analysis, Numer. Heat Transfer A 35 (1999) 859–873.

[11] T.Q. Qiu, C.L. Tien, Femtosecond laser heating of multi-layer metals. I. Analysis, Int. J. Heat Mass Transfer 37 (1994) 2789–2797.

[12] D.Y. Tzou, The generalized lagging response in small-scale and high-rate heating, Int. J. Heat Mass Transfer 38 (1995) 3231–3240.

[13] P.J. Antaki, Importance of nonequilibrium thermal conductivity during short-pulse laser-induced desorption from metals, Int. J. Heat Mass Transfer 45 (2002) 4063–4067.

[14] D.Y. Tzou, K.S. Chiu, Temperature-dependent thermal lagging in ultrafast laser heating, Int. J. Heat Mass Transfer 44 (2001) 1725–1734.

[15] M.A. Al-Nimr, S. Kiwan, Effect of thermal losses on the microscopic two-step heat conduction model, Int. J. Heat Mass Transfer 43 (2001) 1013–1018.

[16] M.A. Al-Nimr, M. Hader, M. Naji, Use of the microscopic parabolic heat conduction model in place of the macroscopic model validation criterion under harmonic boundary heating, Int. J. Heat Mass Transfer 46 (2003) 333–339.

[17] J.K. Chen, D.Y. Tzou, J.E. Beraun, Numerical investigation of ultrashort laser damage in semiconductors, Int. J. Heat Mass Transfer 48 (2005) 501–509.

[18] H. Wang, W. Dai, R. Nassar, R. Melnik, A finite difference method for studying thermal deformation in a thin film exposed to ultrashort-pulsed lasers, Int. J. Heat Mass Transfer 49 (2006) 2712–2723.

[19] H. Wang, W. Dai, R. Nassar, R. Melnik, A finite difference method for studying thermal deformation in a double-layered thin film exposed to ultrashort-pulsed lasers, Int. J. Thermal Sci. 45 (2006) 1179–1196.

[20] H. Wang, W. Dai, L.G. Hewavitharana, A finite difference method for studying thermal deformation in a double-layered thin film with imperfect interfacial contact exposed to ultrashort pulsed lasers, Int. J. Thermal Sci. 47 (2008) 7–24.

[21] M.A. Al-Nimr, O.M. Haddad, V.S. Arpaci, Thermal behavior of metal films—a hyperbolic two-step model, Heat and Mass Transfer 35 (1999) 459–464.

[22] M.A. Al-Nimr, V.S. Arpaci, The thermal behavior of thin metal films in the hyperbolic two-step model, Int. J. Heat Mass Transfer 43 (2000) 2021–2028.

[23] M. Al-Odat, M.A. Al-Nimr, M. Hamdan, Thermal stability of superconductors under the effect of a two-dimensional hyperbolic heat conduction model, Int. J. Numer. Methods Heat Fluid Flow 12 (2002) 173–177.

[24] M. Naji, M.A. Al-Nimr, M. Hader, The validity of using the microscopic hyperbolic heat conduction model under as harmonic fluctuating boundary heating source, Int. J. Thermophys. 24 (2003) 545–557.

[25] M.A. Al-Nimr, M.K. Alkam, Overshooting phenomenon in the hyperbolic microscopic heat conduction model, Int. J. Thermophys. 24 (2003) 577–583.

[26] J.K. Chen, J.E. Beraun, Numerical study of ultrashort laser pulse interactions with metal films, Numer. Heat Transfer A 40 (2001) 1–20.

[27] J.K. Chen, J.E. Beraun, C.L. Tham, Comparison of one-dimensional and two-dimensional axisymmetric approaches to the thermomechanical response caused by ultrashort laser heating, Journal of Optics A: Pure Applied Optics 4 (2002) 650–661.

[28] J.K. Chen, W.P. Latham, J.E. Beraun, Axisymmetric modeling of femtosecond-pulse laser heating on metal films, Numer. Heat Transfer B 42 (2002) 1–17.
[29] J.K. Chen, J.E. Beraun, C.L. Tham, Investigation of thermal response caused by pulsed laser heating, Numer. Heat Transfer A 44 (2003) 705–722.
[30] H.E. Elsayed-Ali, T. Juhasz, Femtosecond time-resolved thermomodulation of thin gold films with different crystal structures, Phys. Rev. B 47 (1993) 13599–13610.
[31] W. Dai, T. Niu, A finite difference scheme for solving nonlinear hyperbolic two-step model in a double-layered thin film exposed to ultrashort-pulsed lasers with nonlinear interfacial conditions, Nonlinear Analysis: Hybrid Systems C 2 (2008) 121–143.
[32] D.Y. Tzou, Macro To Micro Heat Transfer, The Lagging Behavior, Taylor & Francis, Washington DC, 1996.
[33] H. Wang, A finite difference method for studying thermal deformation in two-dimensional micro scale metal thin films exposed to ultrashort pulsed lasers, PhD Dissertation, Louisiana Tech University, LA, 2007.
[34] G.W.C. Kaye, Tables of Physical and Chemical Constants and Some Mathematical Functions, 14th ed., Longman, London, UK, 1973, p. 31.
[35] Y.S. Touloukian, R.W. Powell, C.Y. Ho, P.G. Klemens, Thermal Conductivity, Thermophysical Properties of Matter 1, IFI/Plenum, New York, 1970.